ATLANTIS PRESS

Advances in Computer Science Research, volume 62

2nd Joint International Information Technology, Mechanical and Electronic Engineering Conference (JIMEC 2017)

Study On Static Characteristics Of A Herringbone Grooved Hydrodynamic Journal Bearing: Numerical Simulations

Dewang Chai *, Qian Ding*†, Bin Wang*

* *School of Mechanical Engineering, Tianjin University, Tianjin 300072, China*
† *Tianjin Key Laboratory of Nonlinear Dynamics and Chaos Control, Tianjin 300072, China*

Keywords: herringbone grooved hydrodynamic journal bearing, computational fluid dynamics, Influences of structure parameters.

Abstract

The flow field of a herringbone grooved hydrodynamic journal bearing is numerically simulated by using FLUENT, a computational fluid dynamics software, to reveal the complexity of hybrid oil flowing. Influences of structure parameters on pressure distribution, static characteristics and cavitation are analyzed. Results indicate that the load capacity of bearing increases with the enlarging of spiral angle, reducing of groove depth, increasing of groove number and widening of oil seal margin. The friction moment reduces with the decreasing of groove number and oil seal margin length, and enlarging of groove depth. The maximum friction moment appears as the spiral angle is about π/6. Rate of flow can increase with the increasing of spiral angle and groove depth, and reducing of the grooves number and oil seal margin length. Fewer cavitations can be induced with the increasing of spiral angle, groove depth, and groove number, and narrowing of oil seal margin length.

1 Introduction

Modern machines are increasingly designed in high speed and high power. Sliding bearings are widely used as supporters in high-speed machinery, whose performance has important influence on rotating machinery. The structure of bearing plays a critical role in the performance of bearing. The herringbone grooved bearing, as one style of the spiral oil wedge bearing, being applied more broadly, which could effectively improve the dynamic and thermal characteristics of bearings.

Herringbone groove bearing, with a certain number of herringbone grooves on the surface of oil chamber, can divide the carriage in all directions. The stability and vibration resistance of oil film are improved. Jiankang Wu et al. [1] analyzed the dynamic characteristics of the spiral groove radial sliding bearing using the finite element method, and identified the parameter values in which the stability of oil film is optimized. Hanting Zhu and Qian Ding [2] investigated the static characteristic of herringbone groove bearings via the finite difference method. Influence of the main geometric parameters on the pressure distribution of oil film is revealed.

Currently, both above approaches are widely used to solve the Reynolds equation in various structural bearing researching, but influences of the factors such as inertia term, film curvature and radial flow field impact were neglected. Calculation error was somehow inevitably introduced [3]. Computational Fluid Dynamics (CFD) software can be employed in those areas with complicated structure or more detail analysis is needed. Qingshui Gao et al. evaluated the pressure distribution on ordinary cylindrical bearing and stated the influence on the carrying capability of the bearings which have slots on the housing up and down [4]. Tao Ma et al. used FLUENT software to solve the ordinary four-cylinder chamber oil film pressure and temperature fields [5]. Tianbiao Yu researched the dynamic characteristics on the ultra-high speed grinding hybrid bearing with five chambers via FLUENT software [6]. Lin Tu simulated the force field on plaint bearings also achieve more accurate results by using Fluent software [7].

In this paper, a FLUENT software is used to obtain the static characteristic and bearing pressure distribution of herringbone groove bearings, and the influences of parameters, including spiral angle, depth, number of grooves and oil seal margin length, on the performance of herringbone grooved journal bearing are analyzed. The investigation attempts to provide reference for the design of appropriate supporting structure.

2 Models

2.1 Physical Models

Supposing the groove width is equal to the ridge in circumferential direction, the unfolded drawing of working surface of a herringbone grooved journal bearing (HGJB) is shown in fig.1, in which the shadow parts are grooves. The

spiral angle β is generated between the groove direction and the dimensionless axial coordinates.

The geometry parameters for the bearings are set as: journal eccentricity e=0.1mm, spiral angle β=0~π/3, bearing width L=40mm, bearing diameter D=40mm, oil supply orifice diameter φ=4mm, radial clearance c=0.04mm, groove depth h_g=0.02~0.06mm, the number of grooves n=6~10. According to the symmetry, the half part of the HGJB is established by means of UG software which is shown in fig.2.

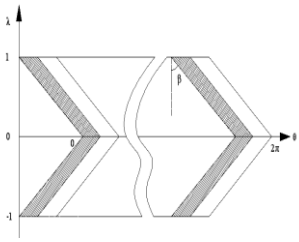

fig.1 Unfolded drawing of working surface of HGJB.

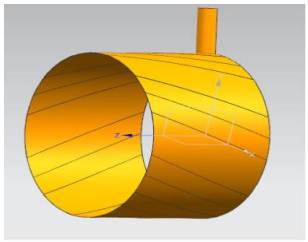

fig.2 Half-width model of HGJB.

2.2 Meshing

The UG modal is imported into ICEM module and the hexahedral structured grid is utilized, which has the better adaptation for complex geometric shape. A good number of grids are required to improve the quality of the grid and capture the characteristics of the details. Mesh of the film of HGJB and the enlarged drawing is shown in fig.3.

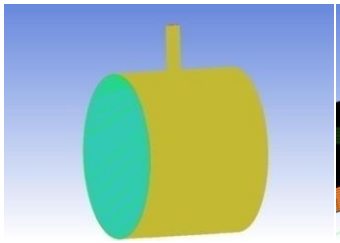

(a) Mesh of the film of HGJB

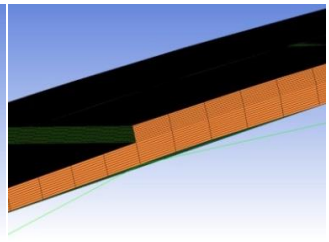

(b) Grid at the end side

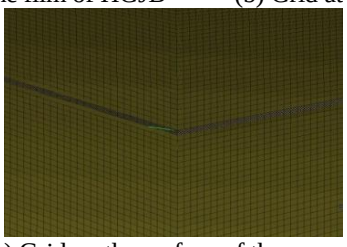

(c) Grid on the surface of the groove

fig.3 Mesh of the film of HGJB and the enlarged drawing in detail

3 Governing Equation

3.1 Mass Conservation Equation

For incompressible flows, the mass conservation equation with constant density is stated as follows:

$$\nabla \cdot (\boldsymbol{v}) = 0 \tag{1}$$

where v is the speed vector.

3.2 Momentum conservation equation

It is also called Navier-Stokes（N-S）equation, that is

$$\nabla \cdot (\rho \boldsymbol{v}\boldsymbol{v}) = -\nabla p + \nabla \cdot (\boldsymbol{\tau}) + \rho \boldsymbol{g} + \boldsymbol{F} \tag{2}$$

where ρ is media density, p pressure, ρg gravity and F the volume force. The stress tensor τ can be written:

$$\boldsymbol{\tau} = \mu[(\nabla \boldsymbol{v} + \nabla \vec{\boldsymbol{v}}^{\mathrm{T}}) - \frac{2}{3}\nabla \boldsymbol{v}\boldsymbol{I}] \tag{3}$$

where μ is fluid viscosity and I is the unit tensor.

3.3 Cavitation model

Cavitation phenomenon is the phase alternation by transferring between the gas and liquid. The mass percentage of the gas f can be described as the gas is increased or decreased, and it meets the following equation

$$\nabla(\rho \boldsymbol{v}_{\mathrm{v}} f) = \nabla(\gamma \nabla f) + R_{\mathrm{e}} + R_{\mathrm{c}} \tag{4}$$

Where ρ is the hybrid density, f is the mass percentage of the gas phase, v_v is the velocity of gas phase, γ is the effective transmission coefficient, R_e, R_c are the generation and disappear rate, respectively.

4 Simulation by Fluent

4.1 The Calculation Model Assumptions

The case has an assumption of constant fluid properties, which is typical in lubrication analysis. The heat exchange between the oil and wall is neglected and the friction heat is taken away by the oil leaking from the both end port along the axil. Temperature-viscosity relations, the heat distortion of bearings or journal and wall slip are not taken into account.

4.2 Simulation Parameter Settings

Import the grid model into FLUENT software, select laminar flow, SIMPLE algorithm and the second order upwind discrete format. Inlet and outlet port are both considered as pressure boundary condition, the inlet pressure is Ps=20KPa, the outlet pressure at both end ports along the axil are ambient pressure, the gauge pressure is equal to 0, dynamic viscosity μ=0.0283Pa.s, the journal spinning speed is set to 2000r/min, the housing is stationary as fixed wall and gasification pressure is Pc= 7650Pa. Let the residual error precision is 10^{-6}, then initial the boundary condition and start iteration meanwhile observe the convergence of the residual curves.

4.3 The oil force field distribution

The parameters β, h_g and n are set to be π/4, 0.06mm and 6, respectively, as the basic case. When the calculation converges, we get the flow field distribution on the herringbone groove bearings under the steady state, as shown in fig.4. We can conclude that, to compare with the plaint bearing, the maximum pressure dose not only focus on the minimum oil film thickness but dispersed in the tip region of the slot, which surrounds the journal more widely.

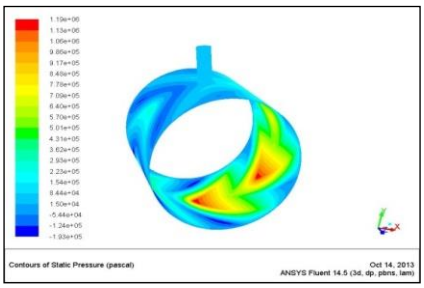

fig. 4 Pressure distribution contours on the bearing surface

Fig.5 shows the static pressure distribution in different cross section of the bearing surface, in which the horizontal axial stands for angle coordinate whose origin is the center of the bearings in Cartesian coordinate with the vertical direction defined 0 rad, positive value in a clockwise direction and negative value in a counter-clockwise direction. Vertical axial is the static pressure value on the bearing surface. One finds that the maximum static pressure appears at the center line section of the bearing, and decreases gradually towards the both ends. The pressure distribution curve shaped as sawtooth has a good agreement with the result in reference [2], obtained using the finite difference method. Some negative pressure values appear in view of cavitation effect.

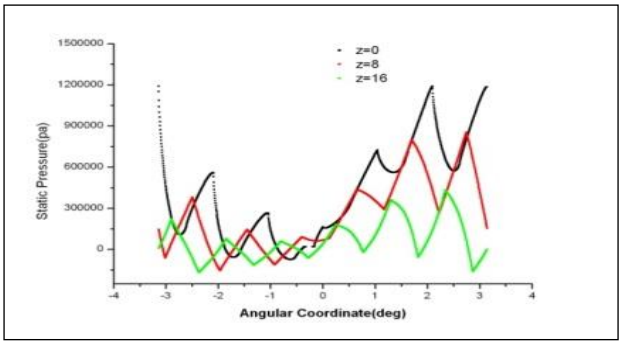

fig. 5 Static pressure distribution in different cross section of the bearing surface

5 The Influence of Structure Parameter

Influences of structure parameters (including spiral angle, depth, number of grooves, oil seal margin length) on pressure distribution, moment of friction, carrying capacity and gas fraction of volume in cavitation will be given and discussed in the following.

5.1 The influence of spiral angle

The influence on pressure distribution

In fig.6, pressure distribution contours on the HGJB surface are displayed with the spiral angles 0, π/6, π/4, π/3, respectively. The corresponding maximum pressure values are 0.548MPa, 1.01MPa, 1.19MPa and 1.27MPa. As the spiral angles increases, the pressure difference between the groove and ribbon becomes larger, the maximum pressure occurs assembly at the centerline of the bearing. Circumferential pressures are totally rising accompany with the spiral angles ascending as shown in fig.7. The extent of the growth between the adjacent spiral angles is declined, increasing by 82%，17.8%，6.7%, respectively. Manufacture processing will be more difficult while enlarging the spiral angle.

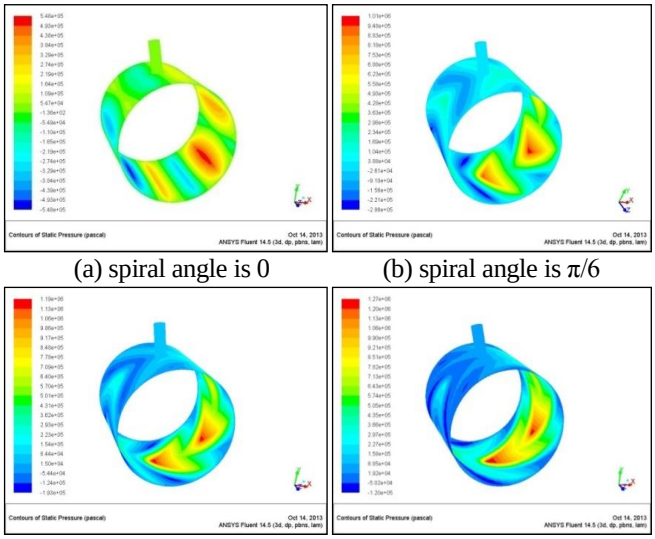

(a) spiral angle is 0 (b) spiral angle is π/6

(c) spiral angle is π/4 (d) spiral angle is π/3

fig. 6 Pressure distribution contours on the HGJB surface with various spiral angles

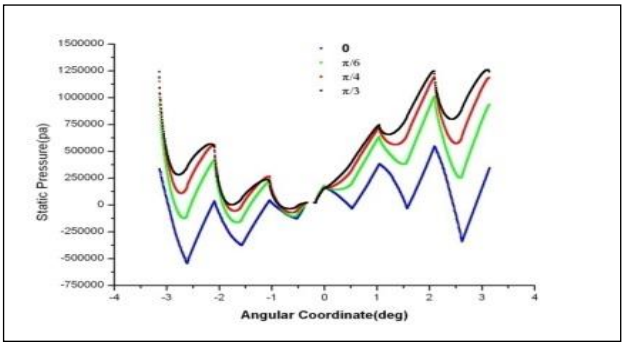

fig. 7 Pressure scatterplot at the centerline of HGJB with various spiral angles

The influence on static characteristic

Fig.8. shows the static characteristic of the HGJB with various spiral angles. The vertical axis So, F, Q stand for dimensionless load capability, dimensionless moment of friction, quality of mass flow, respectively. We can notice that, the carrying capacity is increased with the increasing of the spiral angle, and it increases by 76.8% from the spiral angle 0 to π/3.

The moment of friction firstly increases by 2.5% from 0 to π/6 but decreases by 2.3%, 4.9% from π/6 to π/4 and from π/4 to π/3, respectively. It is indicated that the maximum value of the moment of friction exists nearby π/6.

The oil mass flow is increasing from 0 to π/4, but little decreasing from π/4 to π/3. Totally, both the circumferential and axial mass flow increase with increasing of spiral angle which can make load-carrying assembly and lead the heat dissipation more easily.

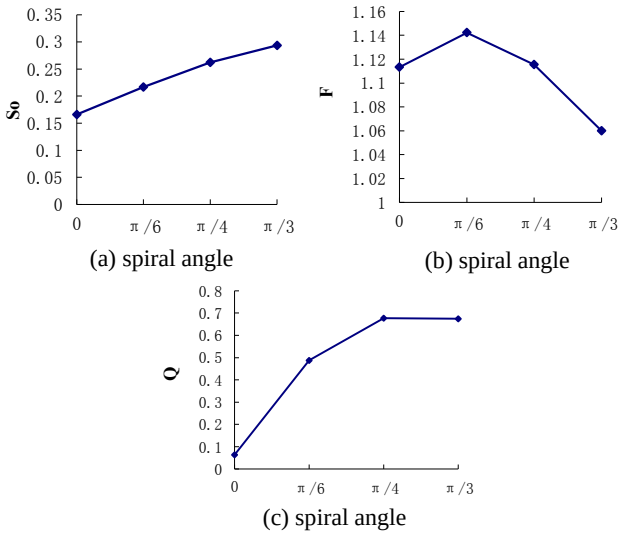

(a) spiral angle (b) spiral angle

(c) spiral angle

fig. 8 Static characteristic figure of the HGJB with various spiral angles

The influence on vapor volume fraction distribution

In Fig. 9, the contour of volume stands for the vapor volume fraction distribution, the color is more closed to red, the more cavitation appears. When the spiral angle is 0, cavitation occurs in the slot along the axial. As the spiral angle goes larger, the cavitation is squeezed outside the groove, and become more narrowly. Little can be seen in the spiral angle π/3 due to the pressure concentration towards the middle line of the bearings.

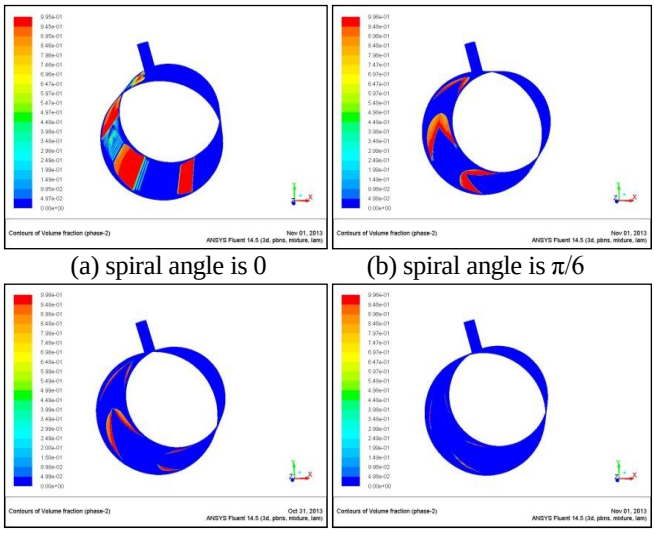

(a) spiral angle is 0 (b) spiral angle is π/6

(c) spiral angle is π/4 (d) spiral angle is π/3

fig.9 Vapor volume fraction distribution of the HGJB with various spiral angles

5.2 The influence of groove depth

The influence on pressure distribution

Fig.10 shows clearly that the maximum pressure values are 1.16MPa, 1.19MPa, 1.07MPa versus the depth of 0.02mm, 0.04mm, 0.06mm, respectively, and occurs nearby the minimum oil thickness at the tip of the groove in the carrying region. From fig. 11, we can also find that in region of carrying area, some of the pressure curves overlap when the depth is 0.02mm and 0.04mm, and drops significantly when the depth is 0.06mm. That results from both the oil thickness and the pressure inward gathering.

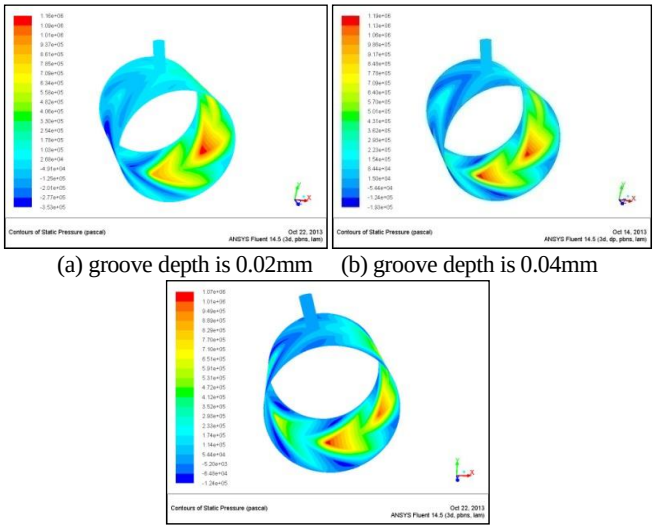

(a) groove depth is 0.02mm (b) groove depth is 0.04mm

(c) groove depth is 0.06mm

fig. 10 Pressure distribution contours on the HGJB surface with various groove depth

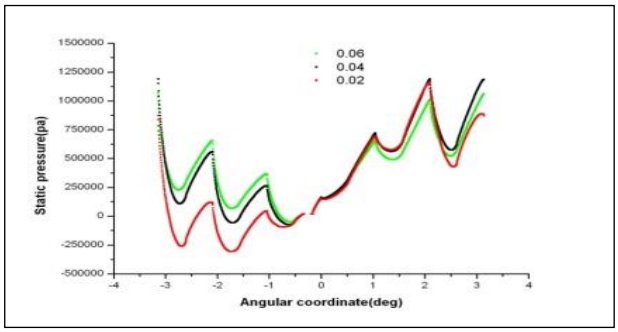

fig.11 Pressure scatterplot at the centerline of HGJB with various groove depth

The influence on static characteristic

Fig.12 presents the static characteristic of the HGJB versus groove depth 0.02mm, 0.04mm, and 0.06mm. One notices that the carrying capacity declines as the rising of the depth, and decreases by 40.3% from 0.02mm to 0.06mm. Generally, the depth of groove is designed less than the clearance between the journal and bearing, otherwise it may reduce the effect of carrying capacity and lubrication. But it is good to heat dissipation in view of the moment of friction dropping and the mass flow increasing. So both the carrying capacity and temperature rise factors should be considered simultaneously to make a choice.

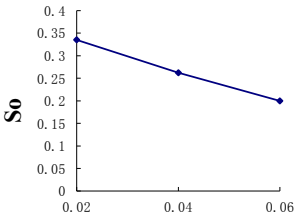

(a) groove depth

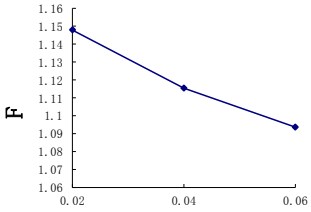

(b) groove depth

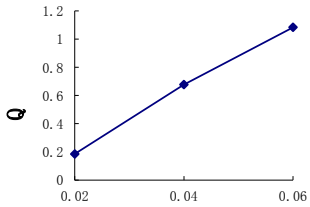

(c) groove depth

fig. 12 Static characteristic figure of the HGJB with various groove depth

The influence on vapor volume fraction distribution

Cavitation shapes as herringbone outside the groove in the non-load region, and distributes more rarely as the increasing of the depth as shown in fig. 13. This can be explained that, the oil contained in the groove can make the lubrication more effectively and lead the pressure distribution relatively stable both the circumferential and axial directions.

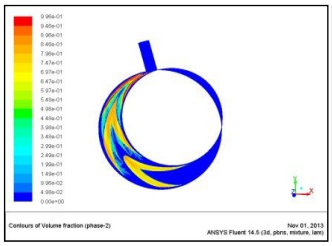

(a) groove depth is 0.02mm (b) groove depth is 0.04mm

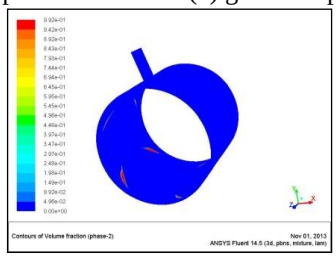

(c) groove depth is 0.06mm

fig. 13 Vapor volume fraction distribution of the HGJB with various groove depth

5.3. The influence of the number of grooves

The influence on pressure distribution

Pressure distribution contours on the HGJB surface with various numbers of grooves are displayed in fig. 14. It can be easily found that the maximum pressure value are 1.21MPa 1.9MPa and 1.20MPa vs. the number of the grooves 6, 8 and 10, respectively. The circumferential and axial pressure varies more gently as the number of grooves increases, which enhances the stability of bearing. That can also be seen clearly in fig. 15, which shows the comparison of pressure distribution at the centerline of HGJB with various numbers of grooves.

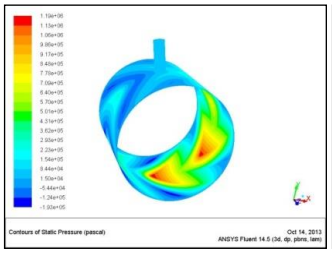

(a) 6 grooves (b) 8 grooves

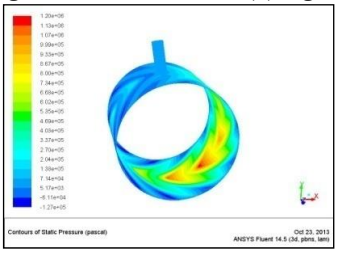

(c) 10 grooves

fig. 14 Pressure distribution contours on the HGJB surface with various numbers of grooves

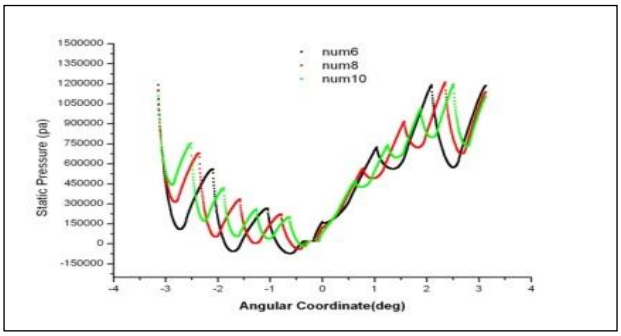

fig. 15 Comparison of pressure distribution at the centerline of HGJB with various numbers of grooves

The influence on static characteristic

Fig. 16 presents the static characteristic of the HGJB with various numbers of grooves. The growth rate between the number of 6, 8 and 10 in load capacity is increased by 1.1% and 0.3%, in moment of friction is increased by 0.6% and 0.1%, and in mass flow is decreased by 0.8% and 0.5%, respectively. Only Large changes occurs from the number 6 to number 8, so add too much number of grooves will increase processing difficulty in exchange for a small amount of bearing capacity improvement. In general, the number of grooves selected about 6 to 12 is appropriate and optimized in engineering.

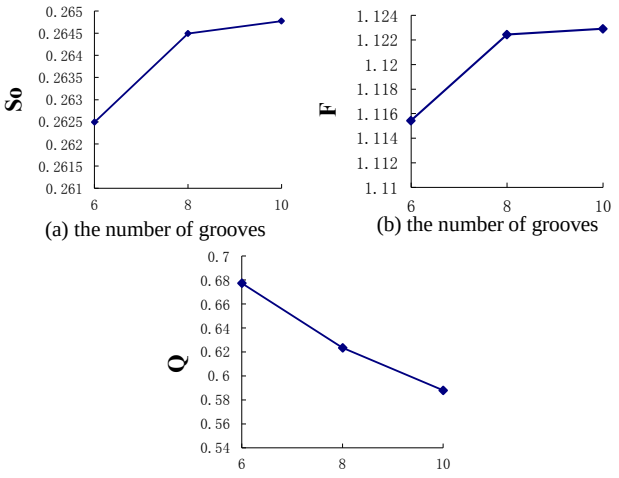

(a) the number of grooves (b) the number of grooves

(c) the number of grooves

fig. 16 Static characteristic figure of the HGJB with various numbers of grooves

The influence on vapor volume fraction distribution

Vapor volume fraction distributions are clearly shown in fig. 17 versus various numbers of grooves, as we can see that cavitation distributing range becomes more narrowly along with the number of grooves increase. The reason is that circumferential and axial pressure changes more smoothly as the number of groove raise.

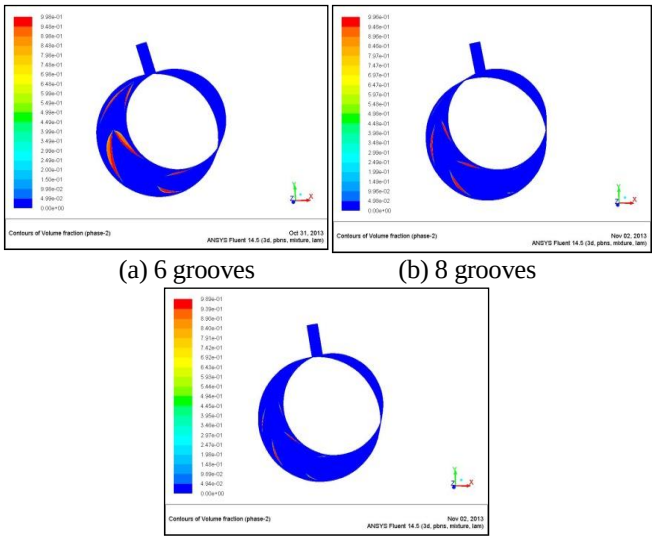

(a) 6 grooves (b) 8 grooves

(c) 10 grooves

fig. 17 Vapor volume fraction distribution of the HGJB with various numbers of grooves

5.4 The influence of oil seal margin length on static characteristic of the HGJB

It also exists the non-through style HGJB in application, whose margin length as oil sealing appears at the both ends of the bearing symmetrically. Fig.18 shows the case that the margin length is a quarter of the width of bearing. Various length of sealing including margin-width ratio 1/4 and 1/2 are discussed compared to the cut-through style.

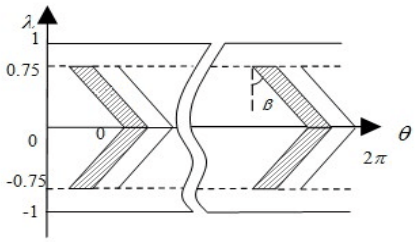

fig.18 Unfold drawing of working surface of the HGJB without cut through

The influence on pressure distribution

According to the contours of static pressure as shown in fig. 19, we note that the maximum pressure value are 1.19MPa，1.23MPa and 1.19MPa versus the margin-width ratio 0, 1/4 and 1/2, respectively. The vortex appears at the rear of the groove in the non-load region due to the leakage prevention by the margin. Fig.20 shows the fluctuating pressure distribution at the centerline of HGJB with various length of sealing side; little changes can be seen in the carrying region, but remarkable in the non-load region. In fact, the flow behavior in

the clearance becomes more complexity owing to the existing of the margin.

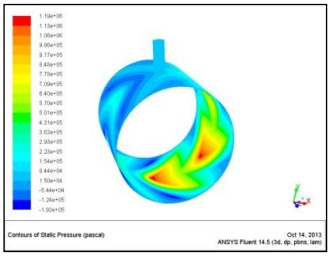

(a) margin-width ratio is 0

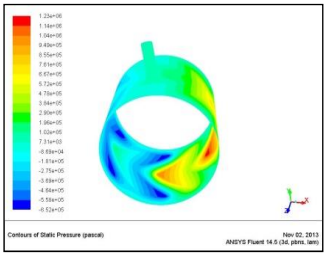

(b) margin-width ratio is 1/4

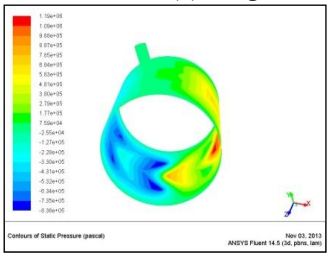

(c) margin-width ratio is 1/2

fig.19 Pressure distribution contours on the HGJB surface with various length of sealing sides

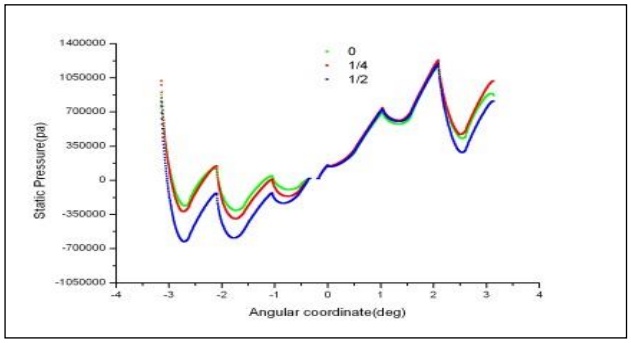

fig.20 Pressure scatterplot at the centerline of HGJB with various length of sealing sides

The influence on static characteristic

Fig.21 presents the static characteristic of the HGJB versus various length of sealing sides. Carrying capability goes up accompanied by enlarging the length of the margin, and the extent increases by 75.1% and 13.6% between the margin-width ratio 0, 1/4, 1/2, respectively. Growth slowing down can be explained as two reasons. On the one hand, margin length increasing reduces the mean clearance, which can lead the carrying capability promoted. On the other hand, the margin length rising may shorten the width of the herringbone grooves, which causes the concentrating inward weakened.

The moment of friction is ascending and the mass flow is declining along with the margin length rising. Both are not good for heat dissipation by oil leaking. Consequently, the margin length needs to be chosen for balancing the carrying capability and heat dissipation.

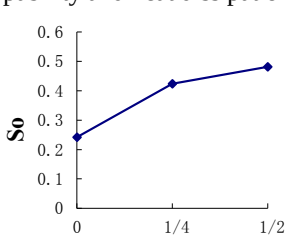

(a) margin-width ratio

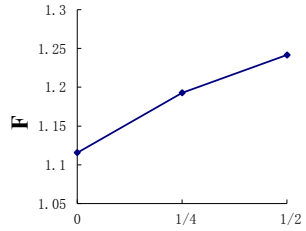

(b) margin-width ratio

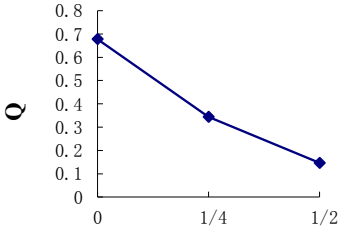

(c) margin-width ratio

fig.21 Static characteristic figure of the HGJB with various length of sealing sides

The influence on vapor volume fraction distribution

As is shown in fig.22, cavitation distribution range becomes wider as the ascending of the margin length, a small amount of which surpass the oil orifice into the load region. That is not expected to see for stability of the HGJB.

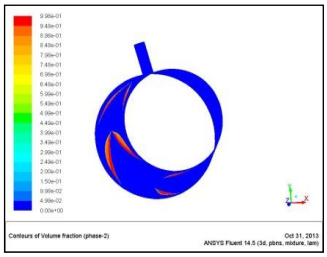

(a) margin-width ratio is 0

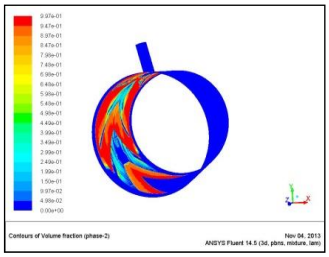

(b) margin-width ratio is 1/4

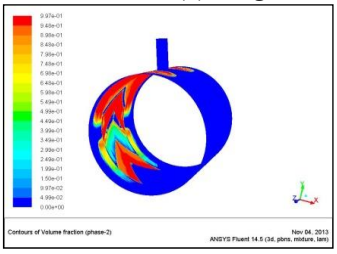

(c) margin-width ratio is 1/2

fig.22 Vapor volume fraction distribution of the HGJB with various numbers of grooves

6 Conclusion

This research investigates the static characteristics of herringbone grooved journal bearing and the influences of

structure parameters such as spiral angle, depth, number of grooves and oil seal margin length on the behavior consisting of pressure distribution, moment of friction, load capacity and gas fraction of volume in cavitations. The following conclusions can be obtained:

(1) The carrying capacity is increased with the increasing of the spiral angle, number of grooves, oil seal margin length and the decreasing of the groove depth. The moment of friction increases with that of the number of grooves, oil seal margin length and the decreasing of the groove depth. The maximum value exists nearby $\pi/6$ in various spiral angles.

(2) Cavitations location moves along with the spinning direction and shapes as herringbone, occurring mostly in the non-load region. Fewer cavitations appear in the case of great spiral angle, deep depth and lots of numbers of grooves.

Acknowledgment

The research is supported by the National Natural Science of China under Grant No. 51575378 and 11502162, and the NSF of Tianjin under Grant No. 13JCZDJC34900 and 15JCQNJC05100.

References

[1] Jiankang Wu, Xiangneng Ma, and Yuying Huang. 1999. "Parameter Comparison Calculations for Oil Film Stability of Grooved Liquid-Lubricated Journal Bearing," *J. Tribology*, 19(1):56-60. (in Chinese)

[2] Hanting Zhu, and Qian Ding. 2012. "Numerical Analysis of Static Characteristics of Herringbone Grooved Hydrodynamic Journal Bearing," *J. Applied Mechanics and Materials*, (105-107):2259-2262.

[3] Shoufeng Huang. 2012. "Research on Static Characteristics of Machine Tool Spindle Hydrodynamic Journal Bearing Based on FLUENT," *D*. Zhengzhou: Zhengzhou University, (in Chinese)

[4] Qingshui Gao, and Jiangang Yang. 2008. "Research on the Dynamic Characteristics of Hydro-dynamical Journal Bearing Based on CFD Analysis," *J. Lubrication Engineering*, 33(9): 65-67. (in Chinese)

[5] Tao Ma, Huiliang Dai, and Siren Liu. 2010. "Numerical Simulation Study on Liquid Hybrid Bearing Based on FLUENT," *J. Journal of Donghua University: Natural Science*, 36(3): 279 -282. (in Chinese)

[6] Tianbiao Yu, Xuezhi Wang, Peng Guan, et al. 2012. "Dynamic Characteristics Analysis on Liquid Hybrid Bearing Based on FLUENT," *J. Lubrication Engineering*, 37 (6):1-5. (in Chinese)

[7] Lin Tu, Duomin Li, and Zihua Duan. 2011. "Pressure Field Numerical Simulation of Hydrodynamic Bearing Based on Fluent," *J. Lubrication Engineering*, 36(4):83-87. (in Chinese)

[8] Zhiming Zhang. 1986. "Theories of hydrodynamic lubrication of sliding bearings," *M*. Beijing: Higher Education Press.